

# Edge reconstruction in the fractional quantum Hall regime

Xin Wan

*National High Magnetic Field Laboratory, Florida State University, Tallahassee, Florida 32310*

E. H. Rezayi

*Department of Physics, California State University, Los Angeles, California 90032*

Kun Yang

*National High Magnetic Field Laboratory and Department of Physics,  
Florida State University, Tallahassee, Florida 32306*

(Dated: October 30, 2018)

The interplay of electron-electron interaction and confining potential can lead to the reconstruction of fractional quantum Hall edges. We have performed exact diagonalization studies on microscopic models of fractional quantum Hall liquids, in finite size systems with disk geometry, and found numerical evidence of edge reconstruction under rather general conditions. In the present work we have taken into account effects like layer thickness and Landau level mixing, which are found to be of quantitative importance in edge physics. Due to edge reconstruction, additional nonchiral edge modes arise for both incompressible and compressible states. These additional modes couple to electromagnetic fields and thus can be detected in microwave conductivity measurements. They are also expected to affect the exponent of electron Green's function, which has been measured in tunneling experiments. We have studied in this work the electric dipole spectral function that is directly related to the microwave conductivity measurement. Our results are consistent with the enhanced microwave conductivity observed in experiments performed on samples with an array of antidots at low temperatures, and its suppression at higher temperatures. We also discuss the effects of the edge reconstruction on the single electron spectral function at the edge.

## I. INTRODUCTION

The edge of a quantum Hall (QH) system provides a special environment to study electron correlations in one dimension. Due to the presence of a strong magnetic field and electron-electron interaction, the bulk of a QH liquid is incompressible, while low-lying excitations exist only at the boundary of the liquid. In an experimental sample, the physics of edge excitations is strongly affected by the interplay of electron-electron interaction and the confining potential due to positive background charge. For example, the edge of an integer QH liquid with a sharp confining potential is described by the chiral Fermi-liquid theory and only a single branch of gapless edge excitations exists due to the presence of magnetic field.<sup>1</sup> When the confining potential is sufficiently smooth, the edge undergoes a reconstruction transition in which a portion of the electron liquid is expelled a few magnetic lengths away from the periphery of the main droplet.<sup>2,3</sup> Additional low-lying edge excitations that propagate in *both* directions arise after the edge reconstruction transition.<sup>3</sup>

The edge excitations of fractional QH liquids are proposed to be described by the chiral Luttinger liquid (CLL) theory.<sup>4</sup> For principal Landau level (LL) filling fractions  $\nu = 1/m$ , the theoretical picture involves only one chiral boson mode. On the other hand our exact diagonalization study<sup>5</sup> of a microscopic model of fractional QH liquids, in finite size systems with disk geometry, suggests that a fractional QH liquid can undergo edge reconstruction for both smooth *and* sharp confining potentials. As a consequence, additional low-energy edge excitations *not* described by the CLL theory are generated and introduce complications into the edge physics. These excitations are clearly visible in the low-energy excitation spectrum of a fractional QH system with reconstructed edge.<sup>5</sup>

Apart from purely theoretical interest and importance, our study of fractional quantum Hall edge reconstruction has also been motivated by two types of experimental studies of edge physics, both with puzzling results. First, the CLL theory predicts a power-law current-voltage dependence ( $I \sim V^\alpha$ ) in the tunneling between a Fermi liquid metal and a QH edge. The prediction has been tested by experiments<sup>6,7,8,9</sup> using samples made by the cleaved-edge overgrowth technique.<sup>10</sup> For a simple filling fraction like  $\nu = 1/3$ , these experiments<sup>6,7,8</sup> found non-Ohmic  $I$ - $V$  dependence with the exponent  $\alpha$  scattering between 2.5 and 2.8, which is close to but noticeably different from the CLL theory prediction of a *universal* exponent  $\alpha = 3$ . Furthermore, no convincing plateau behavior away from  $\nu = 1/3$  is present<sup>7,8</sup> as predicted by the theory. In fact, for  $1/3 < \nu < 1$ ,  $\alpha$  seems to vary continuously for both compressible and incompressible values of  $\nu$ , and no universality in  $\alpha$  can be extracted from data available to date.<sup>7,9</sup> Experimental findings have prompted a number of theories,<sup>11,12,13,14,15,16,17,18</sup> most of which address the continuous dependence of  $\alpha \sim 1/\nu$  found in one experiment<sup>7</sup> only.

The second type of experiments measure the microwave conductivity of a 2DEG with an array of antidots (mi-

croscopic artificial regimes which electrons are forbidden to enter).<sup>19</sup> The microwave conductivity is enhanced with a broad peak centered around  $\nu = 1/2$ , exceeding its dc-value by as much as a factor of 5 for microwave frequencies up to 10 GHz. The enhanced conductivity is suppressed by increasing temperature and disappears for temperature  $T > 0.5$  K. Since the conductivity enhancement and the associated peak are absent for samples without antidots, the effect is believed to be related to the antidot edge excitations coupled to the microwave field. However, from the submicron size of the antidots (with depletion regime diameter 150 - 250 nm) one can easily estimate the usual edge magnetoplasmon modes to have characteristic frequencies above 100 GHz, much higher than the microwave frequencies used experimentally. Therefore, *additional* lower-energy edge excitations are required to interpret the mysterious data.

As we discuss later in the paper, it is likely that both sets of puzzles are related to edge reconstruction and in particular the additional edge modes associated with it. We present further numerical evidence in support of the generality of edge reconstruction in the fractional quantum Hall regime by taking into account effects like layer thickness and Landau level mixing, which are of quantitative importance in edge physics but not considered in our earlier work. We estimate the finite size effects of our numerical studies and find that they have very little effect on our quantitative results of the position of reconstruction transition point. We have also studied in this work the electric dipole spectral function that is directly related to the microwave conductivity measurement and the single electron spectral function, which is what the tunneling experiments measure. Semiquantitative comparison between our results and experiments will be made.

The rest of the paper is organized in the following way. We review our microscopic model in Sec. II. Using heuristic electrostatic calculations, we discuss the origin of the reconstruction of quantum Hall edges and estimate the finite-size effects on microscopic model calculations. In Sec. III we present the numerical evidence for edge reconstruction for boundary conditions describing both sharp and smooth edges. We consider the complications due to LL mixing and finite thickness of the quasi-2D electron layer. Sec. IV studies the effects of thermal fluctuations at finite temperature on edge reconstruction. The relevance of our model and the experimentally observed enhanced microwave conductivity of samples with antidots is discussed in Sec. V, where we present calculations of electric dipole spectral functions. We discuss the effects of the edge reconstruction on the single electron spectral function at the edge of fractional quantum Hall liquids in Sec. VI. We summarize our results in Sec. VII.

## II. MODEL AND ELECTROSTATIC CONSIDERATIONS

We consider a two-dimensional electron gas (2DEG) with disk geometry, as depicted in Fig. 1(a). To model a realistic confining potential, as in a modulation-doped AlGaAs/GaAs heterostructure, we assume the neutralizing background charge is distributed uniformly on a parallel disk at a distance  $d$  above the 2DEG. The radius  $a$  of the positive charge background is so determined that the disk encloses exactly  $N/\nu$  magnetic flux quanta for  $N$  electrons of the 2DEG, for any desired filling factor  $\nu$ . The bare Coulomb interaction between the background charge and the 2DEG gives rise to the confining potential.

Therefore we consider the following Hamiltonian, which describes electrons confined to the lowest LL, using the symmetric gauge:

$$H = \frac{1}{2} \sum_{mnl} V_{mn}^l c_{m+l}^\dagger c_n^\dagger c_{n+l} c_m + \sum_m U_m c_m^\dagger c_m, \quad (1)$$

where  $c_m^\dagger$  is the electron creation operator for the lowest LL single electron state with angular momentum  $m$ .  $V_{mn}^l$  is the matrix element of Coulomb interaction,

$$V_{mn}^l = \int d^2 r_1 \int d^2 r_2 \phi_{m+l}^*(r_1) \phi_n^*(r_2) \frac{e^2}{\epsilon r_{12}} \phi_{n+l}(r_2) \phi_m(r_1), \quad (2)$$

explicitly given by Girvin and Jach<sup>20</sup> for symmetric gauge.<sup>21</sup>  $U_m$  is the matrix element of the rotationally invariant confining potential due to the positive background charge,

$$U_m = \frac{Ne^2}{\pi a^2 \epsilon} \int d^2 r_1 \int_{r_2 \leq a} d^2 r_2 \frac{|\phi_m(r_1)|^2}{\sqrt{r_{12}^2 + d^2}}. \quad (3)$$

Here  $\phi_m$  is the lowest LL wave function

$$\phi_m(z) = (2\pi 2^m m!)^{-1/2} z^m e^{-|z|^2/4}, \quad (4)$$

where  $z = x + iy$  is the complex coordinate in the plane of the 2DEG.

Before we diagonalize the Hamiltonian for microscopic systems to look for evidence of edge reconstruction, we first present a heuristic argument that reveals the electrostatic origin of edge reconstruction. Assuming the electrons are confined by a hard-wall boundary condition at  $r = a$ , we can view the system as a parallel disk capacitor in the electrostatic context, as illustrated in Fig. 1(b). If there is no edge reconstruction, to a good approximation the electron density is uniform from the center of the disk all the way to the edge. Together with the uniform positive background charge, the capacitor is uniformly charged in this case. Within the electron gas layer, the electrostatic potential is a constant in the bulk, but a gradient (or fringe electric field with in-plane component) develops at the edge. This fringe field tends to pull the electrons toward the edge; the distance from the edge over which the fringe field effects are significant is roughly  $d$ . Therefore, the system can gain electrostatic energy by moving electrons *outward* near the boundary along the radial direction. This is expected to happen when the separation between the two oppositely charged disks is large enough. When  $d$  is large, the fringe field effects are strong; thus the electrostatic energy gain from moving some electron density outward at the edge overcomes the associated loss of exchange-correlation energy. We identify this as the driving force of edge reconstruction.

To obtain an estimate of the energetics of this effect, we have calculated the potential energy change of moving one electron from one magnetic length  $l_B = \sqrt{\hbar c/eB}$  (the typical length scale associated with edge reconstruction) inside the edge to the very edge. The energy gain is

$$\Delta E = (2d/l_B) \tan^{-1}(l_B/d) + \ln(1 + d^2/l_B^2), \quad (5)$$

for a half-infinite system, where  $\Delta E$  is in units of  $\nu e^2/\epsilon l_B$ . This energy diverges as  $2 \ln(d/l_B)$  at large  $d$ , as shown in Fig. 2(a). Once this energy gain exceeds the loss of exchange-correlation energy (which must saturate in the large  $d$  limit), edge reconstruction occurs. This calculation demonstrates that edge reconstruction must occur in infinite systems for sufficiently large  $d$  as long as there are states available for electron rearrangements. In addition, it provides an estimate of the energy scale associated with edge reconstruction. It also points to a fundamental difference between the integer and fractional bulks, in the limit of infinite Landau level spacing. For the former, all the possible single electron states are occupied when an infinitely sharp edge is present; thus no reconstruction is possible no matter how large  $d$  is. On the other hand, this is not the case for fractional bulk and reconstruction is guaranteed to occur for sufficiently large  $d$ , despite the presence of a sharp edge boundary.

In this work we perform finite size numerical studies on systems with sizes ranging from 4 to 9 electrons. It is important to ask whether the numerical results presented in this paper reveal the physics in the thermodynamic limit or merely finite-size artifacts. Repeating the above calculation for a finite-size disk capacitor can provide a measure of finite-size effects. The results for systems corresponding to 4 to 9 electrons are shown in Fig. 2(b) for  $d = 2l_B$  (which is close to critical  $d_c$  above which edge reconstruction occurs, say at  $\nu = 1/3$ ). First, we find that the electrostatic energy difference between the edge and one magnetic length inside the edge is very close to the infinite-size value (all within 2%). This suggests the finite-size effect is weak, consistent with our finding that there is essentially no dependence of  $d_c$  on size.<sup>5</sup> Second, finite-size effects *reduce* the electrostatic energy gain and thus work *against* the edge reconstruction. Therefore, we believe that the edge reconstruction we find is robust and not due to finite-size artifacts.

### III. EXACT DIAGONALIZATION STUDY

In this section, we present the ground state properties and low energy excitation spectra of the model Hamiltonian, obtained by exact diagonalization, and look for evidence of edge reconstruction in them. We discuss the appropriate choice of boundary conditions at the edge of the system and show that edge reconstruction is a robust property of the system under different boundary conditions. In particular, we consider the effects of Landau level mixing near the edge due to the presence of a hard-wall potential. We have found that the LL mixing effects, while not of qualitative importance to the edge reconstruction physics, do affect the critical spacing  $d_c$  quantitatively. Our results are also robust in the presence of finite thickness of an electron layer, whose effects turn out to be negligible as long as we treat the electron layer as a sheet of charge at its maximum density.

#### A. Sharp edge

In the previous study,<sup>5</sup> we restricted electrons to  $N/\nu$  orbitals of the lowest LL (*i.e.*, no Landau level mixing), from  $m = 0$  to  $m_{max} = N/\nu - 1$ . Such a constraint was introduced to describe, for filling factor  $\nu$ , the presence of a sharp cleaved edge<sup>10</sup> beyond which electrons cannot move. In the exact diagonalization study, we found, for  $\nu = 1/3$ , the

following evidence that supports the edge reconstruction scenario. (1) The total angular momentum of the global ground state  $M_{tot}$  becomes greater than that of the corresponding Laughlin state when the separation  $d$  between electron and background charge layers exceed critical  $d_c = 1.5 \pm 0.1l_B$ ; the increase of  $M_{tot}$  is due to the outward motion of electrons near the edge triggered by the reconstruction, as discussed in the previous section. The critical value  $d_c$  is essentially the same for  $N = 4-9$  electrons, with very little size dependence. (2) The electron density profile for the global ground state shows significant oscillation near the edge for  $d > d_c$ . (3) Counterpropagating low-lying excitations can be identified in the low-energy excitation spectrum for  $d > d_c$ . We also found that property (2) is present for filling factors  $1/3 \leq \nu \leq 2/3$ , suggesting edge reconstruction is generic for fractional bulk fillings. Properties (1) and (3), on the other hand, are unique to  $1/3$ : (1) because of the existence of the Laughlin state as the reference state and (3) because the single chiral boson mode of the unreconstructed edge does not, in general, extend to other filling factors. So, the mere existence of counter-propagating modes can not be used for general filling factors to look for edge reconstruction. Nevertheless, the general trend remains that  $M_{tot}$  increases with  $d$  for both incompressible and compressible filling fractions, indicating that fractional QH edges tend to reconstruct for large  $d$ . Figure 3 shows the dependence of  $M_{tot}$  on  $d$  for 6, 9, and 12 electrons in 18 orbitals, or  $\nu = 1/3, 1/2$ , and  $2/3$ , respectively. In all three cases,  $M_{tot}$  starts to jump at  $d \sim 1l_B$ .

These numerical findings are consistent with the heuristic arguments that we gave in the previous section. One key quantity in these calculations is the critical  $d$ , which has always been found to be of the order of  $l_B$  (even for the more complicated cases we discuss later in this section). We believe that this is not a coincidence. Within the lowest LL,  $l_B$  is a fundamental length scale which characterizes the size of single electron wave functions. It is thus also the range of effective attraction between electrons due to exchange-correlation effects and therefore the length scale associated with edge reconstruction. On the other hand, the separation between the electron and background charge layers,  $d$ , is the range of the electrostatic fringe field near the edge. Therefore, the electrostatic energy gain generally becomes comparable to the loss of electron exchange-correlation energy when  $d$  is of the order of  $l_B$ ; we thus expect  $d_c \sim l_B$ .

Additional insight into the physics of edge reconstruction may be gained by studying how the low-energy excitation spectrum of the system evolves as  $d$  increases. According to the CLL theory, for simple bulk fillings like  $1/3$ , there exists a single branch of chiral bosonic edge modes with linear dispersion in the long wave-length limit in the absence of edge reconstruction; these modes describe the propagation of the deformation of the periphery of a QH system. This branch of chiral bosonic edge modes is clearly visible in Figure 4, where we show the low-lying spectrum for an  $N = 9$  system at  $\nu = 1/3$  (or,  $m_{max} = 26$ ), for both  $d < d_c$  and  $d > d_c$ . The chirality of the mode is reflected in the fact that low-lying excitations exist only in subspaces  $M > M_0$ , where  $M_0$  is the quantum number of the ground state (which is the same as that of the Laughlin state) for  $d < d_c$ . What is worth emphasizing here are two features not described by the CLL theory. First, the low-lying edge modes, which are clearly separated from the bulk excitations with a gap, exist for relatively large  $\delta M = M - M_0$  (corresponding to large momentum or short wave-length in translationally invariant systems). From the system size we can estimate the momentum  $k = \Delta M / 2\pi R \approx 0.2l_B^{-1}$  for which the mode remains well-defined. Second, the dispersion relation shows significant deviation from linearity and even becomes non-monotonous for larger momenta, with a well-defined local minimum near  $k \approx 0.15l_B^{-1}$ . This non-linearity grows with increasing  $d$ . At  $d = d_c$ , the mode energy crosses zero at this local minimum. Thus the edge reconstruction transition can also be understood as an instability, driven by  $d$ , of the (unreconstructed) chiral boson mode at finite wave vector (of order  $l_B^{-1}$ ). This clearly indicates that edge reconstruction is driven by short-distance physics at the scale of  $l_B$ , in agreement with previous analysis. Based on this insight, a unified field theoretical description for the edges with and without reconstruction, and the transition between the two is advanced by one of us.<sup>22</sup>

As discussed earlier, a cutoff at  $m_{max}$  for single electron states is introduced to model a sharp cleaved edge. Such a sharp edge is not present for all samples. To describe a smooth edge (where confinement is provided only by the positive background), we can move the cut-off to higher angular momentum. In fact, even a sharp cleaved edge is more complicated than imposing a simple cut-off at  $m_{max}$ . More appropriately, electrons are confined in a disk of radius  $a$ , with a very high step-potential at the edge  $r = a$ . The confinement has two related effects. First, the step-potential mixes in high Landau level components for single electron wave functions near the edge and raises the energies for single-particle states, even with angular momentum  $m < m_{max}$  (this is in addition to the effect of the background charge). Second, the change of single-particle wave function, caused by the in-mixing of LLs, changes essentially all the Coulomb interaction matrix elements in Eq. (1). These effects are to be considered in the following subsections.

## B. Smooth edge

As mentioned in the previous subsection, while a sharp cutoff (at  $m_{max}$ ) where the background charge ends describes samples with cleaved edges, it is not present for other samples. Not surprisingly, we find that removing this sharp cutoff can only further favor edge reconstruction. For the 6-electron system considered before,<sup>5</sup> we have increased

the number of orbitals to 30 ( $m_{max} = 29$ ), while keeping the background charge unchanged so that the sharp cutoff is moved about  $2l_B$  away from the boundary of the background charge.<sup>23</sup> Figures 5(a)-(d) show electron densities of the global ground states for  $d = 0.1, 1.6, 2.0,$  and  $5.0$  in the presence of such a smoother edge. Compared with Fig. 1(b)-(e) in Ref. 5, we find that the change of the sharp cutoff has essentially no effect on the electron density for  $d \leq 2.0$ . In particular, the critical distance  $d_c = 1.6$  remains very close to that of the sharp edge case. In these cases, we expect that the electronic states are almost entirely determined by the competition of the electron-electron interaction and the confining potential arising from the background charge. However, with the cutoff moved farther out, the edge piece can shift further away from the disk center for larger  $d$  so that the total momentum  $M_{tot}$  of the lowest ground state increases, e.g. from  $M_{tot} = 65$  to  $105$  for  $d = 5.0$ . Therefore, the inclusion of extra single electron orbitals has very little effect on the edge reconstruction transition; the effects are important only for systems well in the reconstructed phase with  $d \gg d_c$ . For simplicity, in the following discussion we do not include these additional orbitals beyond the boundary of the background charge distribution unless otherwise specified.

### C. Layer thickness

The electrons confined at the interface of the modulation-doped  $\text{Al}_x\text{Ga}_{1-x}\text{As}/\text{GaAs}$  heterostructures, as used in experiments, are not ideally two-dimensional (2D) although their motions perpendicular to the interface are essentially frozen in their ground state due to sharp interface potential. In principle, one needs to use the self-consistently calculated wave function appropriate for the heterostructures to study the softening of electron-electron interaction due to finite electron layer thickness. However, Stern and Das Sarma<sup>30</sup> showed that the Fang-Howard variational wave function,<sup>29</sup>

$$Z_0(z) = 2(2b)^{-3/2} z e^{-z/2b}, \quad (6)$$

is a very good approximation to the numerical self-consistent ground state. The Fang-Howard wave function  $Z_0(z)$  peaks at  $z_0 = 2b$ . The parameter  $b$  gives the scale of the layer thickness, which is typically  $\sim 50 \text{ \AA}$ . The finite layer thickness weakens the electron-electron interaction, as well as the background charge confining potential. For instance, the effective electron-electron interaction in the quasi-2D system is approximated by

$$V(|\vec{r}_1 - \vec{r}_2|) = \frac{e^2}{\epsilon} \iint dz_1 dz_2 \frac{|Z_0(z_1)|^2 |Z_0(z_2)|^2}{[r^2 + (z_1 - z_2)^2]^{1/2}}, \quad (7)$$

where  $r$  is the in-plane distance between two electrons.

For typical experimental parameters, the electron wave functions have a finite thickness  $2b \sim 100 \text{ \AA}$ , equal to roughly one magnetic length. For an  $\text{AlGaAs}/\text{GaAs}$  heterojunction, we choose the  $z$ -direction pointing from the  $\text{AlGaAs}$  to the  $\text{GaAs}$  with the  $\text{AlGaAs}/\text{GaAs}$  interface placed right at the  $z = 0$  plane. Since the  $\text{AlGaAs}$  introduces a potential barrier, the quasi-2D electron density spreads essentially in the  $\text{GaAs}$ . The background charge layer, introduced by  $\delta$ -doping, is thus located at the  $z = -d$  plane (on the  $\text{AlGaAs}$  side). Experimentally,  $d \sim 800 \text{ \AA}$  or above. One central question, therefore, is whether the edge reconstruction persists in the presence of the finite layer thickness; in particular, whether  $d_c$  for the edge reconstruction remains smaller than the typical  $d$  used in experiments. To answer this, we repeat exact diagonalization calculations for several values of  $b$ , searching for the critical  $d$  above which the global ground state has a larger total angular momentum than that of the corresponding Laughlin state. In this calculation, we use a sharp cutoff ( $m_{max} = N/\nu - 1$ ) in the angular momentum space and do not consider the complication of LL mixing. Figure 6 summarizes the results for  $N = 4-9$  electrons for  $\nu = 1/3$ . Again,  $d_c$  is almost size-independent for  $N = 4-9$  electrons, confirming that finite-size effects are weak in this calculation. Overall,  $d_c$  decreases as  $b$  increases, and can be roughly fit by

$$d_c = d_c^0 - 2b, \quad (8)$$

where  $d_c^0 = 1.4 \pm 0.1$ . Note  $d_c$  decreases slightly faster than  $2b$  for small  $b$ ; thus  $d_c^0$  is smaller than  $d_c = 1.5 \pm 0.1$ , which is found for systems with zero thickness. Since  $2b$  is the distance between the  $\text{AlGaAs}/\text{GaAs}$  interface and the peak of the Fang-Howard wave function, an alternative interpretation of the results is that  $d_c$  remains roughly as a constant, if we measure  $d$  from the background charge layer to the plane of maximum electron density, instead of the interface. Thus the overall effect of finite layer thickness favors edge reconstruction, and reduces the critical dopant layer distance  $d_c$  slightly.

$N$	5	6	7	8	9
$d_c$	0.4	1.6	0.6	0.9	1.0

TABLE I:  $d_c$  for edge reconstruction for  $\lambda = (e^2/\epsilon l_B)/\hbar\omega_c = 1.0$ . We define  $d_c$  as the distance at which  $M_{tot}$  of the global ground state exceeds the corresponding value in the  $d \rightarrow 0$  limit.

#### D. Hard-wall confinement and Landau level mixing near the edge

So far, we have been working in the limit where the kinetic energy is completely quenched, so electrons are entirely in the lowest LL. In this limit, the Coulomb energy  $e^2/\epsilon l_B$  is the only energy scale in the system. However, for typical  $n$ -type GaAs heterostructures in experiments, the Coulomb energy is comparable to the cyclotron energy  $\hbar\omega_c$  separating the LLs. For the fractional QH effect, the LL mixing effects have been considered in numerical as well as analytical studies.<sup>24,25,26,27</sup>

The LL mixing effects are important for edge physics, since the single particle energy for electrons confined in a disk increases monotonically from bulk to edge and eventually crosses higher LL energies due to confinement, as first discussed by Halperin<sup>28</sup> in the QH context. Therefore, LL mixing, in particular, resulting from the cleaved sample edge may as well alter the edge physics. To include this effect, we solved the Schrödinger equation for non-interacting electrons confined in a two-dimensional disk (we neglect the finite thickness of the electron layer) by a hard-wall boundary condition:

$$\psi(r) = 0, \text{ for } r > a. \quad (9)$$

The ground state wave function  $\psi_m^{gs}(r)$  in each angular momentum ( $m$ ) subspace now becomes a mixture of states in all LLs with the same  $m$  quantum number. As a result, the energy of the ground states increases from  $\hbar\omega_c/2$  (lowest LL value) for  $m = 0$  to approach  $3\hbar\omega_c/2$  (first LL value) for  $m_{max} = 3N - 1$ , as depicted in Fig. 7(b) (here we do not include contributions from the confining potential of the background charge). Figure 7(a) shows the cumulative overlaps,  $\sum_{i=0}^n |\langle \psi_m^{gs}(r) | \phi_m^i(r) \rangle|^2$ , of the corresponding ground state wave functions  $[\psi_m^{gs}(r)]$  for each angular momentum  $m$ , with the LL wave function  $[\phi_m^i(r)]$  for the lowest five LLs ( $i = 0-4$ ). The total overlap of the five lowest LLs is more than 99% for each  $m$ .

Following the usual procedure of projecting the Hamiltonian of the system onto the ground state manifold, we obtain an effective Hamiltonian in the same form as Eq. 1, with  $c_m^\dagger$  creating an electron in the LL-mixed ground state with angular momentum  $m$ . The single particle wave functions  $\phi_m$  in Eq. (2) and (3) are replaced by  $\psi_m^{gs}$ . We absorb the  $m$ -dependent single-particle energy  $\epsilon_m$  into the confining energy term  $U_m$ . We restrict the Hilbert space to  $0 \leq m < 3N$  for  $\nu = 1/3$ . Note that we have, in addition to  $e^2/\epsilon l_B$ , a second energy scale  $\hbar\omega_c$ . The LL mixing effect is thus characterized by the dimensionless parameter  $\lambda = (e^2/\epsilon l_B)/\hbar\omega_c$ . We are, in particular, interested in  $\lambda \sim 1$ , which is close to the real experimental conditions. The LL mixing raises  $\epsilon_m$  by roughly  $\hbar\omega_c$  for edge states, thereby making electrons occupying these states energetically unfavorable. However, the squeezing of the wave functions near the edge due to the Landau level mixing effect lowers the confining potential from the background charge and also reduces the range of effective attraction due to exchange-correlation effects. These effects favor edge reconstruction.

Figure 8 shows the low-energy spectra for  $N = 9$  electrons in 27 orbitals with hard-wall boundary conditions for various  $d$  and  $\lambda = 2.0$ . After edge reconstruction, the total ground state momentum becomes  $M_{tot} = 116$ , increasing from  $M_{tot} = 108$  of the corresponding Laughlin state. Counterpropagating low-energy modes can be observed near  $M_{tot} = 116$  for  $d = 1.5l_B$ . Qualitatively, these results agree very well with the scenario using sharp cutoff in angular momentum space (Fig. 4). However, we also observe fluctuations in the critical  $d_c$  for systems with different sizes. For  $\lambda = 1.0$ , we list  $d_c$  in Table I, which varies from  $0.4 l_B$  to  $1.6 l_B$ . Although the data seems to stabilize at  $d_c \approx 1.0$ , we cannot draw definitive quantitative conclusions without data from larger systems in contrast to the case of no LL mixing. We believe the increased finite size effect here is due to the fact that LL mixing affects states in a relatively wide region near the edge; this effect was not present in our earlier study. We also point out that here we define  $d_c$  as the distance at which  $M_{tot}$  exceeds the corresponding value in the  $d \rightarrow 0$  limit and the results presented are based on this working definition. With strong LL mixing effects, the ground state for  $d < d_c$  may not have an  $M_{tot}$  consistent with the value of the corresponding Laughlin state. We believe that such a different  $M_{tot}$  in the limit of  $d \rightarrow 0$  suggests the Laughlin state may not be a good approximation to the ground state. In other words, we probably cannot identify the finite systems as having filling fraction  $1/3$  unambiguously.

We would like to emphasize that all of our numerical results, as well as the heuristic arguments based on electrostatic considerations, suggest that  $d_c \sim l_B$ . In real samples, on the other hand,  $d \gtrsim 10l_B$ . We thus believe that it is safe to conclude that the edges of all samples studied so far are reconstructed when the bulk filling is fractional, regardless

of whether the edges are cleaved or not.

#### IV. EFFECTS OF FINITE TEMPERATURE ON EDGE RECONSTRUCTION

Thus far our studies have been focusing on ground state (or zero temperature) properties of the system, especially those related to edge reconstruction. It is of interest to investigate how finite temperature, and the thermal fluctuations associated with it, affect these properties. In our previous study,<sup>5</sup> we used a finite-temperature Hartree-Fock approximation to show that the reconstruction of a  $\nu = 1$  QH edge is suppressed above a certain temperature  $T^*$ . This is quite reasonable since thermal fluctuations tend to suppress edge density oscillations associated with reconstruction. In that study the temperature  $T^* \approx 0.05e^2/\epsilon l_B$  (or  $T^* \approx 6$  K) for typical experimental parameters. It is expected, however, that the Hartree-Fock calculation tends to overestimate the temperature scale, due to effects of finite size, layer thickness, LL mixing, disorder, etc. Here we study the effects of finite  $T$  for fractional bulk filling  $\nu = 1/3$ . In this case a Hartree-Fock calculation is no longer possible; we thus use exact diagonalization to generate all the excited states with significant thermal weight and perform thermal averaging. Figure 9 shows the evolution of the density profile for 7 electrons at  $\nu = 1/3$  at several temperatures. We find that, similar to what we found earlier for  $\nu = 1$ , the edge density oscillation associated with edge reconstruction is washed out above a certain characteristic temperature,  $T^* \approx 0.05e^2/\epsilon l_B$ , at which the density profile no longer has strong oscillations and becomes quite similar to that of the corresponding Laughlin state. This is about the same temperature scale (but for much smaller systems) that we got for the integer edge from Hartree-Fock; we expect the temperature scale will become much lower for a comparable size system.

#### V. MICROWAVE CONDUCTIVITY AND ITS TEMPERATURE DEPENDENCE

The microwave conductivity related to microwave absorption of our microscopic system can be calculated through the electric dipole spectral function as follows:

$$\sigma(\omega) \propto \sum_{i \rightarrow f} |\langle \psi_f | \hat{e} \cdot \vec{r} | \psi_i \rangle|^2 \delta(E_f - E_i - \hbar\omega) f(E_i) (E_f - E_i), \quad (10)$$

where  $f(E) = e^{-E/k_B T}/Z$  is the thermal weight of a state with energy  $E$ .  $E_{i,f}$  and  $\psi_{i,f}$  are the energies and wave functions for initial and final states, respectively, and the summations are over all eigenstates.  $\hat{e}$  is the unit vector of an electric field and  $\vec{r}$  the position vector for electrons.

The microwave conductivity, as determined from Eq. (10) for a system of 6 electrons for  $\nu = 1/3$  at different temperatures, both before ( $d = 1.0l_B$ ) and after edge reconstruction ( $d = 2.0l_B$ ), are shown in Figs. 10(a) and (b). The data is coarse-grain averaged in frequency space for clarity of viewing. For  $d = 1.0l_B$ , the spectral function shows a dominant peak at  $\omega \approx 0.04$ , in units of  $e^2/\hbar\epsilon l_B$ . This peak corresponds to the single chiral edge mode for the principal filling factor  $\nu = 1/3$ , marked by a solid arrow in the corresponding excitation spectrum, Fig. 10(c). At higher temperature, the peak becomes less prominent, due to the reduced statistical weight of the ground state and other low-lying states; however the position of the peak does not shift with changing  $T$ , and the peak can still be identified as the dominant one in the whole spectrum for temperature up to  $T = 0.05$ , in units of  $e^2/\epsilon l_B$ . For  $d = 2.0l_B$ , where edge reconstruction has occurred, the frequency dependence of the conductivity becomes qualitatively different. Two distinct peaks can be resolved for  $\omega < 0.05$  at  $T = 0.01$ , contributed by three dominant modes, with two in the lower peak (marked by a dotted arrow and a dashed arrow). The additional modes are due to edge reconstruction, which creates two counter-propagating edge modes. What is more interesting is the manner in which the conductivity evolves as  $T$  increases; here we find, at higher temperatures, the peak of the spectral function *shifts* to higher frequencies, and the low frequency response due to the additional modes get *suppressed*. The low-temperature peaks can barely be resolved at  $T = 0.05$ . Such behavior is in good qualitative agreement with the microwave experiments in samples with an array of antidots (reported in Ref. 19). These authors find enhanced low frequency (much lower than the edge magneto plasmon frequency) conductivity at low  $T$ , while such enhancement gets suppressed at higher  $T$ . One should note, however, that the system size of our study (as, say, parameterized by the circumference of the edge) is much smaller than those of the real samples; thus, not surprisingly, the energy and temperature scales obtained in our work is considerably larger than those of the experimental data; this is purely a finite size effect. On the other hand the temperature scale obtained here is consistent with what we obtained in the previous section through the temperature dependence of edge density oscillation.

The microwave experiment on samples with antidots<sup>19</sup> suggests that the observed enhanced conductivity is a generic feature for all fractional filling factors and peaks around  $\nu = 1/2$ . Unfortunately, finite-size effects do not make it

possible for us to obtain conclusive results for arbitrary  $\nu$ , except for simple cases such as  $\nu = 1/3$ . This is because the hierarchy FQH states have more complicated edge structure, which necessarily leads to stronger finite-size effects; the situation is even worse for compressible bulk like that of  $\nu = 1/2$ , because the gapless bulk and edge excitations are inevitably mixed together. Here we discuss another relatively simpler case,  $\nu = 2/3$ , where the QH liquids can be understood as a  $\nu = 1/3$  hole condensate embedded in a  $\nu = 1$  electron condensate.<sup>31,32,33,34</sup> Therefore, two counterpropagating edge modes exist even without the edge reconstruction. We find, not surprisingly, these two modes ( $\Delta M = M_{tot} - M_0 = \pm 1$ ) in our numerical calculation for  $d = 0.1$ , as shown in Figs. 11(a) and (c). One mode ( $\Delta M = 1$ , marked by a solid arrow) has a squared dipole matrix element almost two orders of magnitude larger than the other ( $\Delta M = -1$ , marked by a dotted arrow), so the low-temperature spectral function is dominated by a single mode (the edge magnetoplasmon mode). On the other hand, for  $d = 2.0$ , we find, more edge modes which include two  $\Delta M = -1$  low-energy excitations as shown in Fig. 11(d). These new modes can roughly be regarded as the results of the edge reconstruction of the inner  $\nu = 1/3$  hole condensate. There is no evidence that the outer  $\nu = 1$  edge can be reconstructed since we model samples with sharp cleaved edges. The dipole spectral function, however, is now dominated by one of the  $\Delta M = -1$  modes [marked by a solid arrow in Fig. 11(c)], with a squared spectral weight more than two orders of magnitude greater than those of the  $\Delta M = 1$  modes (the lowest one marked by a dotted arrow). Thus, quite similar to the  $\nu = 1/3$  case, we find additional modes due to edge reconstruction at larger  $d$ . We also find the transition processes that dominate the dipole spectral function and microwave conductivity change due to edge reconstruction. Also similar to the  $\nu = 1/3$  case, the dipole spectral function becomes dominated by bulk excitations at high temperatures and the low-frequency spectral weight gets suppressed. Thus the calculation of the dipole spectral function at  $\nu = 2/3$  also finds additional low-energy modes generically arise from the reconstruction of fractional QH edges, and they make important contribution to the low-frequency dipole spectral function. Such contribution, however, get suppressed at high temperatures. Thus this behavior is not specific to principal bulk filling, in agreement with the enhanced microwave conductivity in antidot samples in the entire fractional filling range, and its suppression at higher temperature.

## VI. SINGLE ELECTRON SPECTRAL FUNCTION AND EDGE TUNNELING

Numerical calculations of single electron spectral function at the edge in finite size systems have been performed by Palacios and MacDonald.<sup>35</sup> They considered a QH droplet with Coulomb interaction, but without a physically realistic confining potential. In particular, they calculated the squared matrix elements between the ground state of an  $N$ -electron system to the low-lying states of the corresponding  $(N + 1)$ -electron system at  $\nu = 1/3$ . These numerical results can be compared to those obtained by the CLL theory, which predicts that the low-lying energy spectrum of a QH system at principal filling fraction, such as  $\nu = 1/3$ , can be described by a branch of single-boson edge states with angular momentum  $l$  ( $l = 1, 2, 3, \dots$ ) and energy  $\epsilon_l$ . In the CLL language, we can label each low-energy state by a set of occupation numbers  $\{n_l\}$ , whose total angular momentum and energy are  $M = M_0 + \Delta M = M_0 + \sum_l l n_l$  and  $E = E_0 + \Delta E = E_0 + \sum_l n_l \epsilon_l$ , respectively, where,  $M_0$  and  $E_0$  are total angular momentum and energy of the corresponding ground state. Palacios and MacDonald<sup>35</sup> found excellent agreement between the squared matrix elements,  $T(\{n_l\}) = |\langle \psi_{\{n_l\}}(N + 1) | c_{3N + \Delta M}^\dagger | \psi_0(N) \rangle|^2$ , calculated numerically in the microscopic model and those calculated based on the CLL theory. Note that  $M_0(N + 1) - M_0(N) = 3N$  is the difference in total angular momenta between the  $N$ - and  $(N + 1)$ -electron ground states. Such a comparison is made possible by the unambiguous identification of the low energy spectrum in terms of  $\{n_l\}$  (based on  $\Delta M$  and  $\Delta E$ ), as well as in the agreement of the corresponding values of  $T(\{n_l\})$ , at least for  $M \leq 4$ .

In this section, we study the single electron spectral function in the presence of a physically realistic edge confining potential, generated by a layer of background charge, distributed uniformly on a disk at distance  $d$  above the 2DEG. As discussed earlier, the single electron spectral function is directly measured in edge tunneling experiments. We are interested in finding out how the electron spectral function is affected by the presence of the edge confining potential, which mixes the eigenstates in the system without the confinement. In particular, we are interested in whether and how the electron spectral function is affected by edge reconstruction.

We calculated the tunneling spectral weights for  $\nu = 1/3$  by adding one more electron into a system of 6 electrons. The realistic edge confining potential is generated by the appropriate background charge, which neutralizes the resulting system. For  $d = 1.0$  (before reconstruction), we plot the spectrum and electron spectral weights in Fig. 12(a) and (b), respectively. As in the absence of the confining potential, we can identify the lowest edge excitations for each  $M = M_0 + \Delta M$  subspace in the low-energy excitation spectrum as the single-boson edge state with  $n_l = \delta_{l, \Delta M}$  (with excitation energy  $\epsilon_l$ ). Thus, the family of edge states can be unambiguously identified, since their  $\Delta M$  and  $\Delta E$  must be simultaneously written as linear combinations of  $l$  and  $\epsilon_l$ , respectively. We list the tunneling spectral weights for  $\Delta M \leq 4$  in Table II, which are highlighted by solid lines in Fig. 12. These matrix elements are rather close to those obtained in the absence of the confining potential,<sup>35</sup> and consistent with the predictions of the CLL theory (for



		d = 1.0		d = 1.6		
		(no reconstruction)		(with reconstruction)		
$\Delta M$	$\{n_l\}$	$\Delta E$	$T(\{n_l\})$	$\Delta E$	$T(\{n_l\})$	CLL theory
0	{0000}	0.0000	1.000	0.0000	1.000	1
1	{1000}	0.0317	2.791	0.0241	2.845	3
2	{2000}	0.0631	3.772	0.0477	4.074	4.5
	{0100}	0.0434	1.383	0.0314	1.681	1.5
3	{3000}	0.0943	3.288	0.0714	4.480	4.5
	{1100}	0.0738	3.863	0.0559	3.644	4.5
	{0010}	0.0461	0.734	0.0306	1.320	1
4	{4000}	0.1252	2.083	0.0972	3.413	3.375
	{2100}	0.1038	5.182	0.0797	5.113	6.75
	{1010}	0.0756	2.529	0.0535	4.312	3
	{0200}	0.0853	0.587	0.0621	0.955	1.125
	{0001}	0.0465	0.402	0.0266	0.839	0.75

TABLE II: Tunneling spectral weights  $T(\{n_l\}) = |\langle \psi_{\{n_l\}}(N+1) | c_{3N+\Delta M}^\dagger | \psi_0(N) \rangle|^2$ , for microscopic model at  $\nu = 1/3$ , before ( $d = 1.0l_B$ ) and after ( $d = 1.6l_B$ ) edge reconstruction transition (normalized to the ground state-to-ground state matrix element,  $T_0$ ), and for CLL theory. The microscopic system contains  $N = 6$  electrons with corresponding background charge before an additional electron tunnels into the electron layer.  $\Delta M = M - M_0$  and  $\Delta E = E - E_0$  (in units of  $e^2/\epsilon l_B$ ) are total angular momentum and energy measured from the corresponding ground state values ( $M_0$  and  $E_0$ ) for the resulting system.  $\{n_l\}$  is a set of occupation numbers of the bosonic edge-wave with angular momentum  $l$  and energy  $\epsilon_l$ .

infinite system).

For reconstructed edges on the other hand, the situation becomes more complicated since there are additional nonchiral boson excitations, all of which are coupled in general. However, it has been proposed<sup>3</sup> that in the strong coupling limit (for the unscreened long-range Coulomb interaction which has logarithmic singularity in the long-wave length limit) one mode, which represents the total charge density mode, may dominate and behaves just like the single branch below the edge reconstruction transition. For  $d = 1.6$  (after reconstruction), we plot the tunneling spectrum and spectral weights in Fig. 12(c) and (d), respectively. For the lowest two states with  $\Delta M = +1$ , we find that the squared tunneling matrix element for the lower state is 0.213 and for the second lowest state is 2.845; this is close to 3 which is predicted for the {1000} mode in the CLL theory. For this reason, we may identify the two states as members of the neutral mode and the charge mode, respectively (also the charge mode is indeed expected to have higher energy). In addition, we find that the corresponding squared matrix elements for the ground states in  $\Delta M = 2$ -4 subspaces are 1.681, 1.320, and 0.839, respectively. These numbers are close to 1.5, 1, and 0.75 predicted for the edge modes in the corresponding subspaces. So these three states may be identified as {0100}, {0010}, and {0001} of the charge mode. If the distinction of charge and neutral modes can be made in this way and the charge mode indeed controls the tunneling behavior, we should be able to generate a family of excitations with angular momenta and energies which can be calculated according to the four charge excitations identified so far. We should also be able to find, near the calculated energies in the corresponding angular momentum subspace, excitations with squared matrix elements close to the predictions in the CLL theory. This indeed seems to be the case, as shown in Table II. The listed states are, again, highlighted in Fig. 12. We emphasize that the squared matrix elements for the rest of the low-lying states ( $\Delta E < 0.05e^2/\epsilon l_B$ ) with  $\Delta M \neq 0$  are typically very small, with the largest one being roughly unity (or the ground state-to-ground state value). We point out that in order to calculate the matrix elements for up to  $\Delta M = +4$ , we use a smooth edge with  $m_{max} = 23$ . We found that reducing  $m_{max}$  (giving a sharper edge) has no significant effects on the squared matrix elements in the reduced subspaces. Our results thus suggest that the effect of edge reconstruction on the structure of the single electron spectral function is fairly weak; this is consistent with the experimental finding that the tunneling exponent is close to the prediction of the CLL theory at  $\nu = 1/3$ , despite the fact that the edges are expected to be reconstructed.

## VII. CONCLUSIONS

In this paper, we have performed exact diagonalization studies on microscopic models of fractional QH liquids in systems with disk geometry, and investigated the interplay between electron-electron interaction and confining potential due to background charge near the edge. We have shown that the edges of fractional QH liquids reconstruct when the background charge (dopant) layer is separated far enough from the electron layer, and the critical distance for this to happen is of order one magnetic length. The edge reconstruction happens because the electrostatic energy gained by moving electrons outward near the sample edge increases logarithmically as the separation increases, and eventually exceeds the loss of electron exchange-correlation energy. Such behavior is found to have very weak finite-size effects in most cases, even for small systems with 6-9 electrons that we used in our studies. Our results suggest that edge reconstruction occurs rather generically in high-quality AlGaAs/GaAs samples used in experimental studies, as the corresponding distance in these samples are typically of the order of ten magnetic lengths or larger.

In our studies we have used different types of boundary conditions for electronic wave functions near the edge, corresponding to different types of samples (*e.g.*, whether edge is cleaved or not). We have demonstrated that the edge reconstruction phenomenon is not sensitive to the choices of specific boundary conditions qualitatively, be it hard-wall confinement or one that leads to a smooth confining potential. While different boundary conditions lead to quantitatively different critical spacing between dopant and electron layers, our conclusion that real samples are all in the reconstructed regime is robust.

With reconstructed edges, fractional QH liquids can have additional edge modes that propagate along both directions. In general, we find these modes tend to have much lower energy scales than the edge modes in the absence of edge reconstruction. Therefore, they can have very important effects on the low-energy behavior of edge transport and tunneling experiments. We have performed calculations on the electric dipole spectral function as well as single electron spectral function, for systems with and without edge reconstruction. We find that edge reconstruction affects the dipole spectral function rather strongly, and its frequency as well as temperature dependences compare favorably with microwave conductivity measurements performed in samples with an array of antidots (and their associated edges). On the other hand we find the electron spectral function at  $\nu = 1/3$  is not modified strongly by edge reconstruction; this is consistent with tunneling experiments which find the tunneling exponent at  $\nu = 1/3$  quantitatively close to the prediction of the chiral Luttinger liquid theory, despite the presence of edge reconstruction.

## Acknowledgments

We have benefited from a very informative discussion with Matt Grayson on Landau level mixing near a sharp cleaved edge. We also thank Juan Jose Palacios for helpful correspondences on the calculation of single electron spectral function. This work was supported by NSF grants DMR-9971541 and DMR-0225698 (XW and KY), DMR-0086191 (EHR), the State of Florida (XW), and the A. P. Sloan Foundation (KY).

- 
- <sup>1</sup> B. I. Halperin, Phys. Rev. B **25**, 2185 (1982).
  - <sup>2</sup> A. H. MacDonald, S. R. E. Yang, and M. D. Johnson, Aus. J. Phys. **46**, 345 (1993).
  - <sup>3</sup> C. de C. Chamon and X.-G. Wen, Phys. Rev. B **49**, 8227 (1994).
  - <sup>4</sup> X.-G. Wen, Int. J. Mod. Phys. B **6**, 1711 (1992).
  - <sup>5</sup> X. Wan, K. Yang, and E. H. Rezayi, Phys. Rev. Lett. **88**, 056802 (2002).
  - <sup>6</sup> A. M. Chang, L. N. Pfeiffer, and K. W. West, Phys. Rev. Lett. **77**, 2538 (1996).
  - <sup>7</sup> M. Grayson, D. C. Tsui, L. N. Pfeiffer, K. W. West, and A. M. Chang, Phys. Rev. Lett. **80**, 1062 (1998).
  - <sup>8</sup> A. M. Chang, M. K. Wu, C. C. Chi, L. N. Pfeiffer, and K. W. West, Phys. Rev. Lett. **86**, 143 (2001).
  - <sup>9</sup> M. Hilke, D. C. Tsui, M. Grayson, L. N. Pfeiffer, and K. W. West, Phys. Rev. Lett. **87**, 186806 (2001).
  - <sup>10</sup> L. N. Pfeiffer, K. W. West, H. L. Stormer, J. Eisenstein, K. W. Baldwin, D. Gershoni and J. Spector, Appl. Phys. Lett. **56**, 1697 (1990).
  - <sup>11</sup> S. Conti and G. Vignale, J. Phys. Condens. Matt. **10**, L779 (1998).
  - <sup>12</sup> J.H. Han and D.J. Thouless, Phys. Rev. B **55**, 1926 (1997).
  - <sup>13</sup> U. Zülicke and A.H. MacDonald, Phys. Rev. B **60**, 1836 (1999).
  - <sup>14</sup> D.-H. Lee and X.-G. Wen, cond-mat/9809160 (unpublished).
  - <sup>15</sup> A. Lopez and E. Fradkin, Phys. Rev. B **59**, 15323 (1999).
  - <sup>16</sup> L. S. Levitov, A. V. Shytov, and B. I. Halperin, Phys. Rev. B **64**, 075322 (2001).
  - <sup>17</sup> V. J. Goldman and E. V. Tsiper, Phys. Rev. Lett. **86**, 5841 (2001); E. V. Tsiper and V. J. Goldman, Phys. Rev. B **64**, 165311 (2001).
  - <sup>18</sup> S. S. Mandal and J. K. Jain, Phys. Rev. Lett. **89** 096801 (2002).

- <sup>19</sup> P. D. Ye, *et al.*, Phys. Rev. B **65**, 121305 (2002).
- <sup>20</sup> S. M. Girvin and T. Jach Phys. Rev. B **28**, 4506 (1983).
- <sup>21</sup> Here we assume the layer thickness is zero. Finite layer thickness will be considered later.
- <sup>22</sup> K. Yang, cond-mat/0302344 (unpublished).
- <sup>23</sup> In our numerical studies such a cutoff that is pushed some distance away from the edge is necessarily for having a finite dimensional Hilbert space.
- <sup>24</sup> D. Yoshioka, J. Phys. Soc. Jpn. **55**, 885 (1986).
- <sup>25</sup> V. Melik-Alaverdian and N. E. Bonesteel, Phys. Rev. B **52**, R17032 (1995).
- <sup>26</sup> V. Melik-Alaverdian, N. E. Bonesteel, and G. Ortiz, Phys. Rev. Lett. **79**, 5286 (1997).
- <sup>27</sup> G. Murthy and R. Shankar, Phys. Rev. B **65**, 245309 (2002).
- <sup>28</sup> B. I. Halperin, Phys. Rev. B **25**, 2185 (1982).
- <sup>29</sup> F. F. Fang and W. E. Howard, Phys. Rev. Lett. **16**, 797 (1966).
- <sup>30</sup> F. Stern and S. D. Sarma, Phys. Rev. B **30**, 840 (1984).
- <sup>31</sup> X. G. Wen, Phys. Rev. Lett. **64**, 2206 (1990).
- <sup>32</sup> A. H. MacDonald, Phys. Rev. Lett. **64**, 222 (1990).
- <sup>33</sup> M. D. Johnson and A. H. MacDonald, Phys. Rev. Lett. **67**, 2060 (1991).
- <sup>34</sup> C.L. Kane, M.P.A. Fisher and J. Polchinski, Phys. Rev. Lett. **72**, 4129 (1994).
- <sup>35</sup> J. J. Palacios and A. H. MacDonald, Phys. Rev. Lett. **76**, 118 (1996).

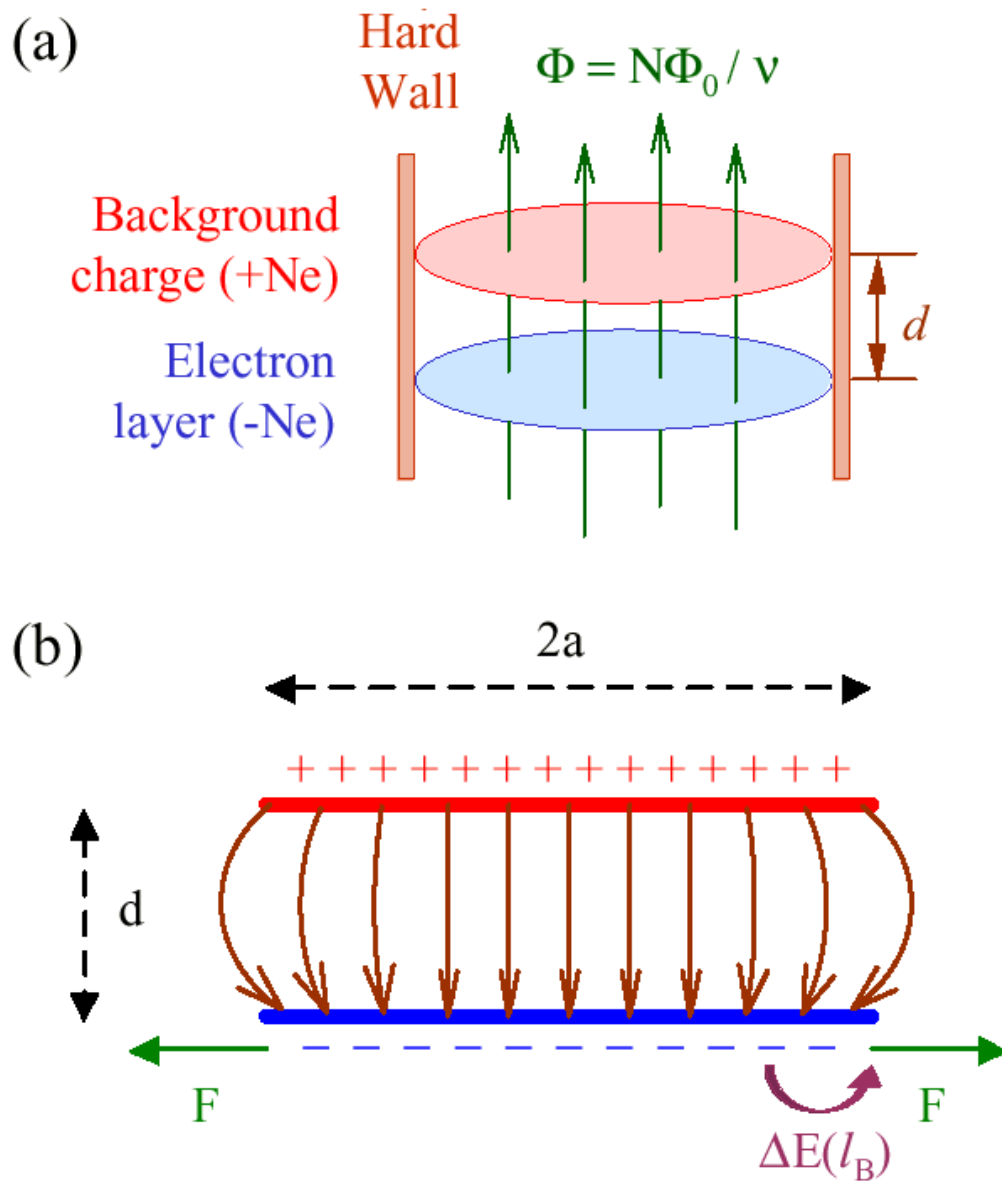


FIG. 1: (a) Sketch of the system with rotational symmetry considered here, which is made of an electron layer and a uniformly distributed, neutralizing background charge layer separated by a distance  $d$  from each other. Electrons are confined by a hardwall boundary condition, so they cannot move beyond the edge of the background charge. (b) The side view of the system. If electrons are uniformly distributed, the electrostatic potential is a constant in the bulk of the electron layer, but a gradient (or fringe electric field with in-plane component) develops at the edge, which tends to pull the electrons toward the edge.

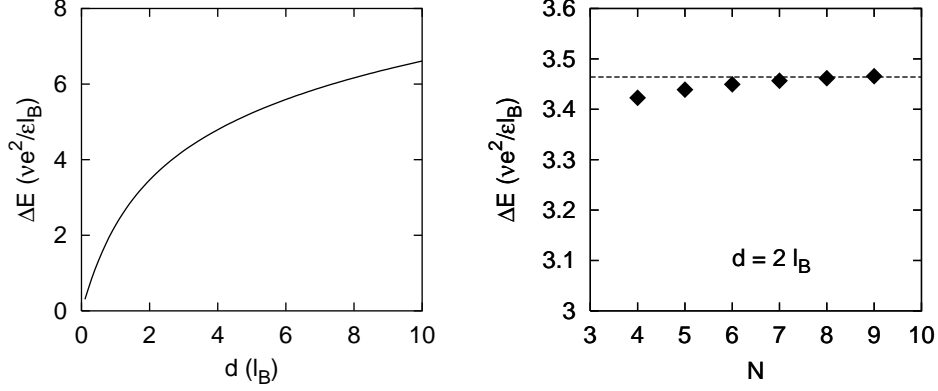


FIG. 2: Estimate of electrostatic energy associated with edge reconstruction and finite size effects. Consider a parallel disk capacitor with uniformly distributed positive and negative charges. Left panel shows the potential energy gain [ $\Delta E = (2d/l_B) \tan^{-1}(l_B/d) + \ln(1 + d^2/l_B^2)$ ] in moving an electron from one magnetic length ( $l_B$ ) inside the edge to the edge, for a half-infinite capacitor system (the infinite-size limit of the disk system).  $d$  is the distance between the two charge layers. Right panel shows  $\Delta E$  in finite-size disk systems (4-9 electrons), with  $d = 2l_B$ , at  $\nu = 1/3$ . The dashed line is the infinite-size limit for  $\Delta E$  at  $d = 2l_B$ .

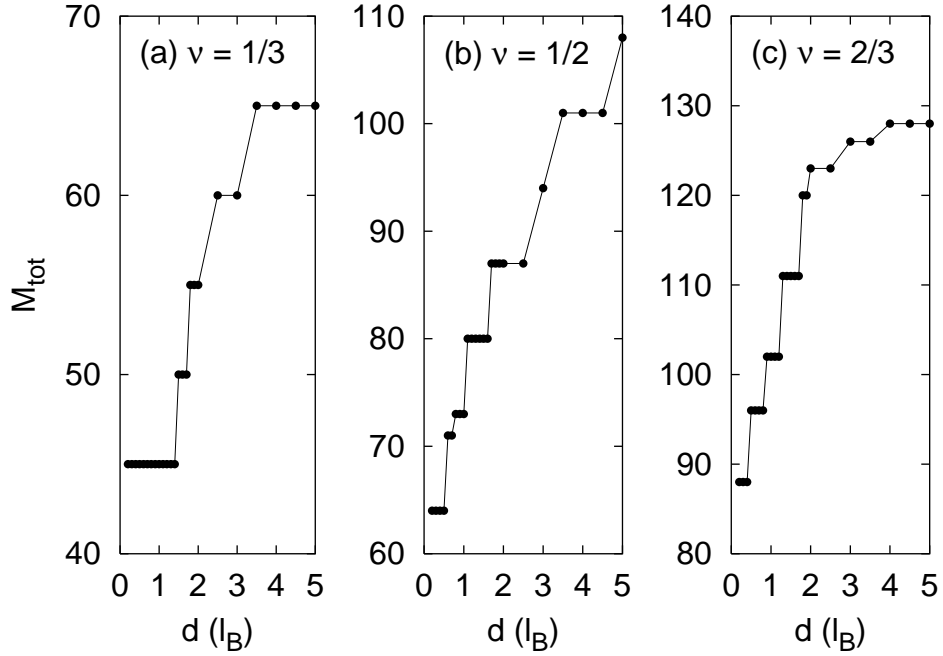


FIG. 3: Dependence of  $M_{tot}$  on  $d$  for 6, 9, and 12 electrons in 18 orbitals, which correspond to  $\nu = 1/3$ ,  $1/2$ , and  $2/3$ , respectively.

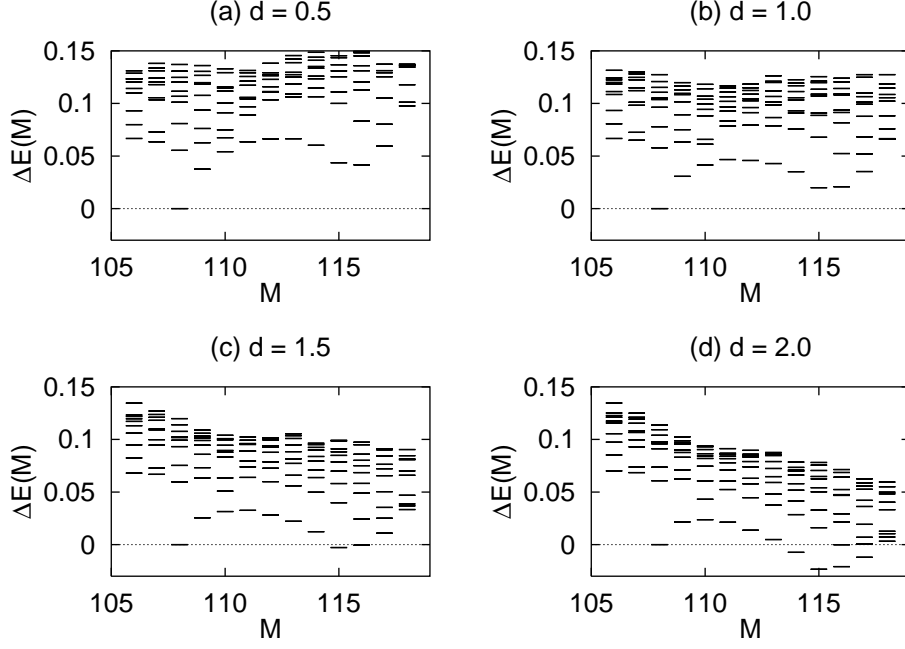


FIG. 4: Low energy spectra for  $N = 9$  electrons in 27 orbitals for (a)  $d = 0.5$ , (b)  $d = 1.0$ , (c)  $d = 1.5$ , and (d)  $d = 2.0$ , in units of  $l_B$ . Excitation energies ( $\Delta E$ ) are measured, in units of  $e^2/\epsilon l_B$ , from the ground state in the  $M_{tot} = 108$  (that of the corresponding Laughlin state) subspace. The edge reconstruction transition occurs around  $d = 1.5$ , as  $\Delta E$  becomes negative for  $M_{tot} = 115$ .

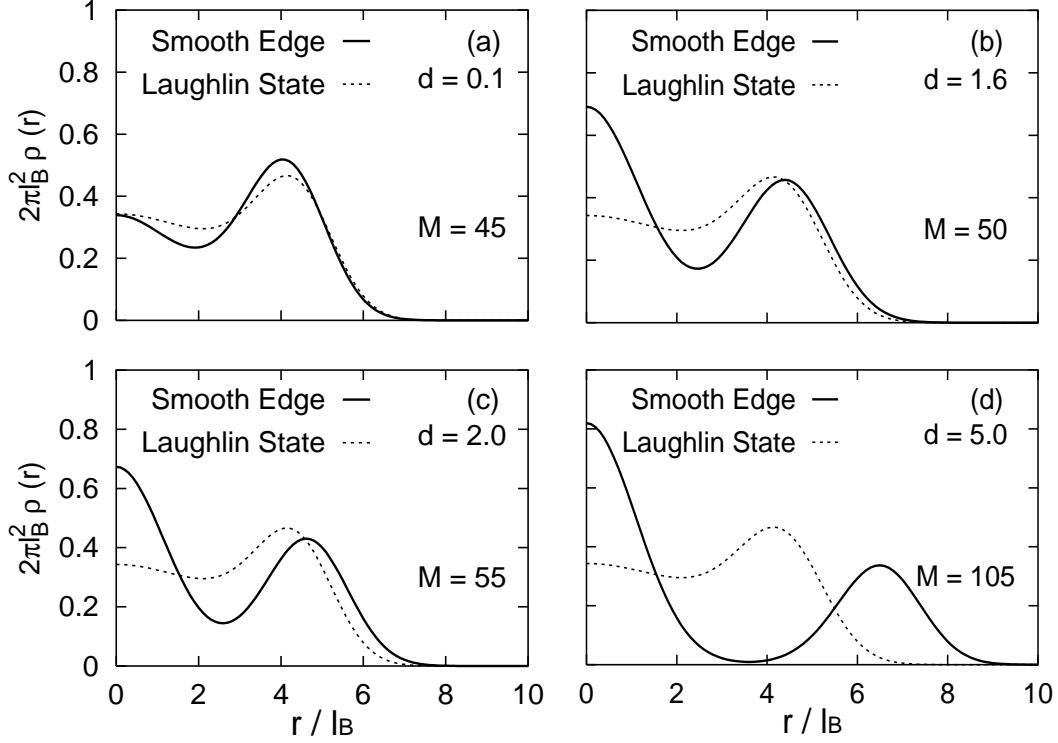


FIG. 5: The electron density  $\rho(r)$  of the global ground state for 6 electrons in 30 orbitals compared with that of the Laughlin state (dotted lines) for (a)  $d = 0.1$ , (b)  $d = 1.6$ , (c)  $d = 2.0$ , and (d)  $d = 5.0$ , in units of  $l_B$ . The radius of the disk with uniform background charge corresponds to  $\nu = 1/3$ , so electrons are allowed to move  $\sim 2l_B$  beyond the background charge.

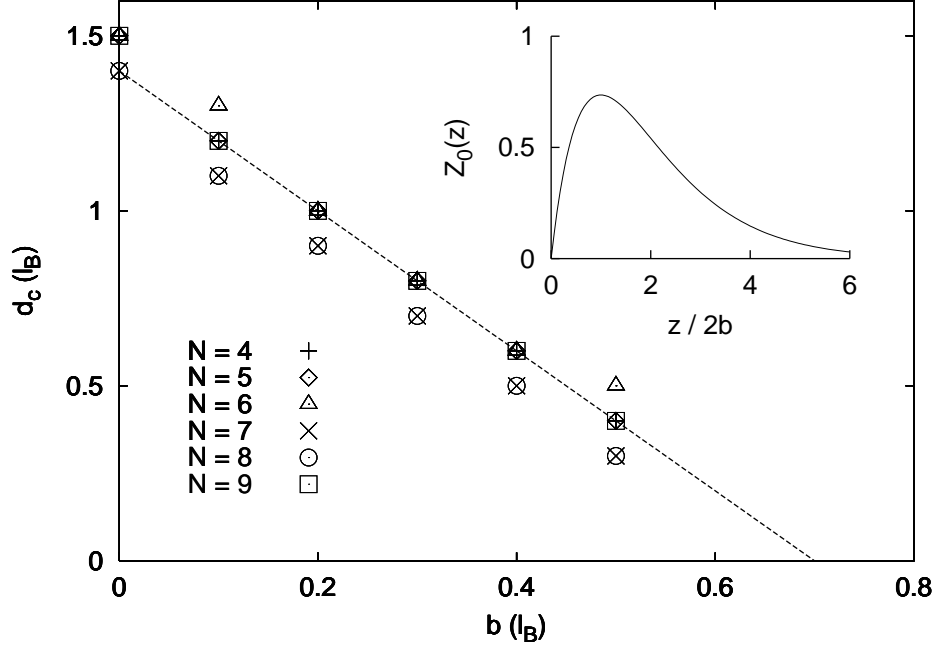


FIG. 6: Critical  $d_c$  (in units of  $l_B$ ) for edge reconstruction, at which the ground state momentum  $M_{tot}$  becomes greater than that for the corresponding Laughlin state, for  $N = 4-9$  electrons at  $\nu = 1/3$  with finite layer thickness.  $d_c$  is measured as the distance from the positive background charge layer to the (GaAs/AlGaAs) interface where potential is discontinuous. The finite thickness of the 2D electron gas in the perpendicular direction is described by the Fang-Howard variational wave function  $Z_0(z) = 2(2b)^{-3/2} z e^{-z/2b}$  (see inset).  $d_c$  can be roughly fit to  $d_c = 1.4 - 2b$ , where  $1.4 \pm 0.1$  can be regarded as the critical  $d$  for zero layer thickness, and  $2b$  the distance from the peak of the variational wave function to the interface ( $z = 0$ ).

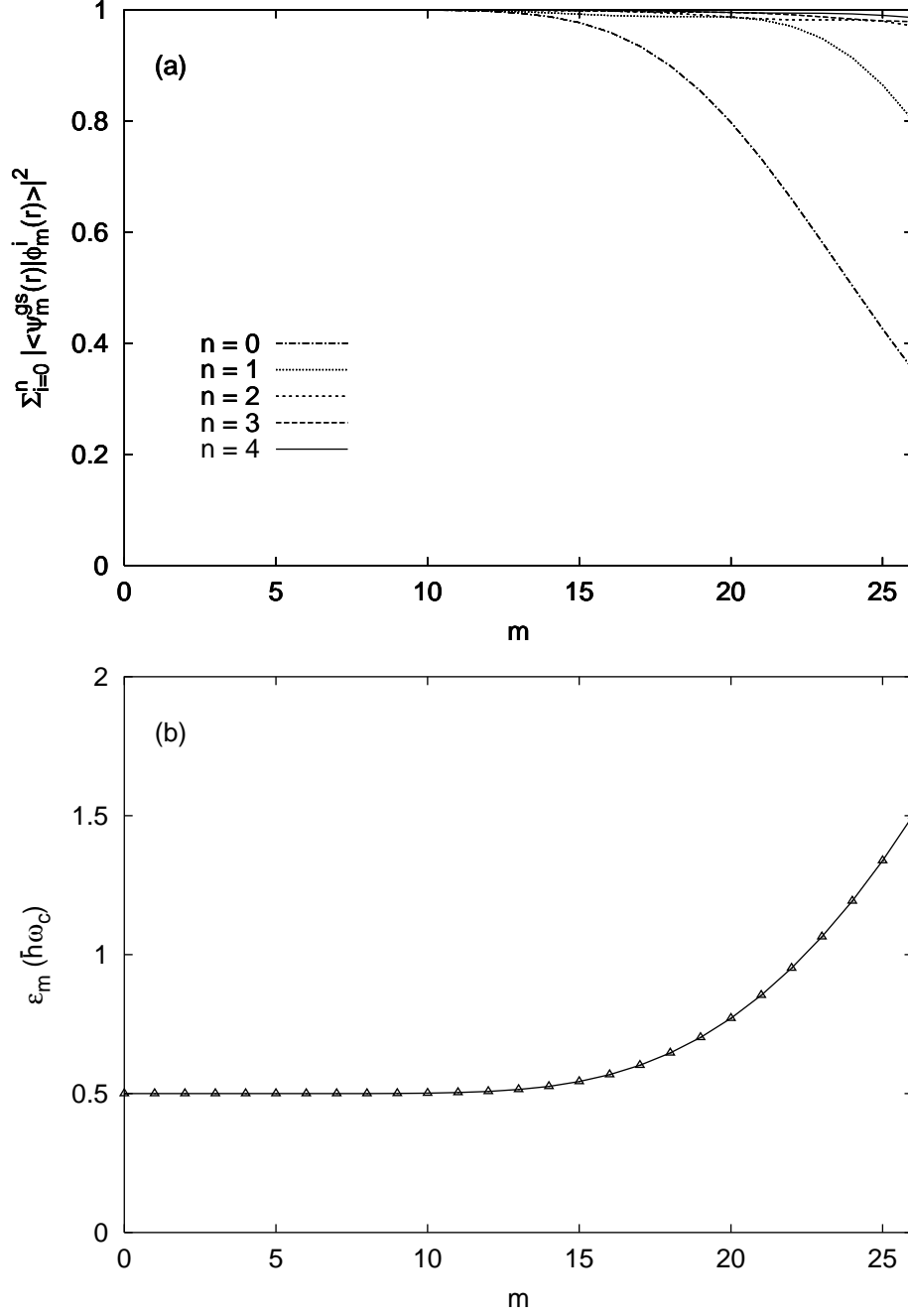


FIG. 7: (a) Cumulative overlaps,  $\sum_{i=0}^n |\langle \psi_m^{gs}(r) | \phi_m^i(r) \rangle|^2$ , of the ground state wave function  $[\psi_m^{gs}(r)]$  for each angular momentum  $m$ , in the presence of a hard-wall boundary condition, with LL wave function,  $\phi_m^i(r)$ , for the lowest five LLs ( $i = 0-4$ ). The sum of the overlaps is more than 99% for each  $m$ . (b) The single-particle energy of the ground state  $\epsilon_m$  increases from  $\hbar\omega_c/2$  in the bulk to  $3\hbar\omega_c/2$  at the edge.



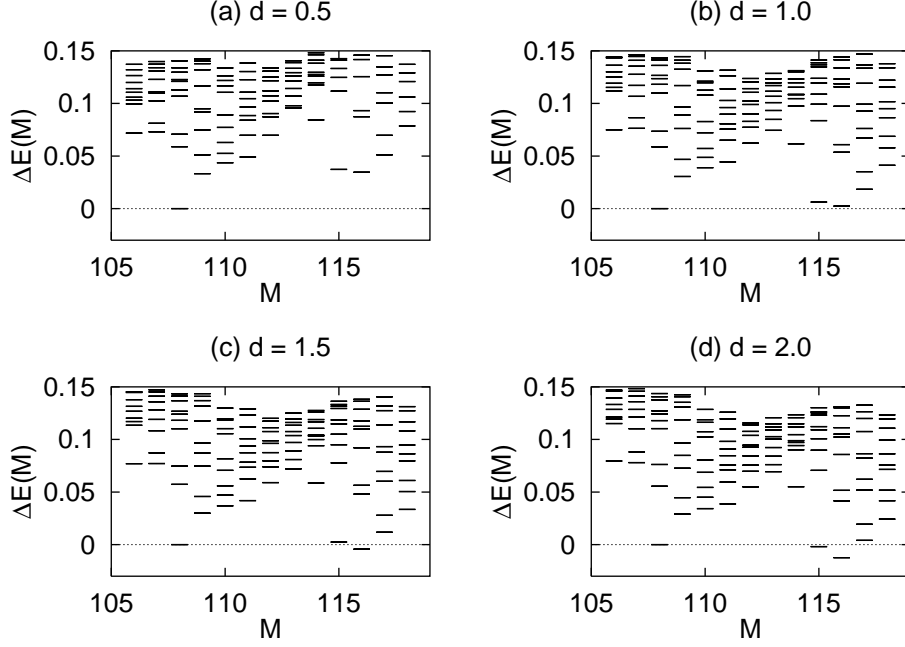


FIG. 8: The low energy spectra for  $N = 9$  electrons in 27 orbitals with hard-wall boundary conditions for (a)  $d = 0.5l_B$ , with no edge reconstruction, (b)  $d = 1.0l_B$ , close to but before edge reconstruction, (c)  $d = 1.5l_B$ , and (d)  $d = 2.0l_B$ , both after edge reconstruction. Excitation energies ( $\Delta E$ ) are measured, in units of  $e^2/\epsilon l_B$ . We choose the dimensionless parameter  $\lambda = (e^2/\epsilon l_B)/\hbar\omega_c = 2.0$  here. After edge reconstruction, the total ground state momentum becomes  $M_{tot} = 116$ , increasing from  $M_{tot} = 108$  of the corresponding Laughlin state.

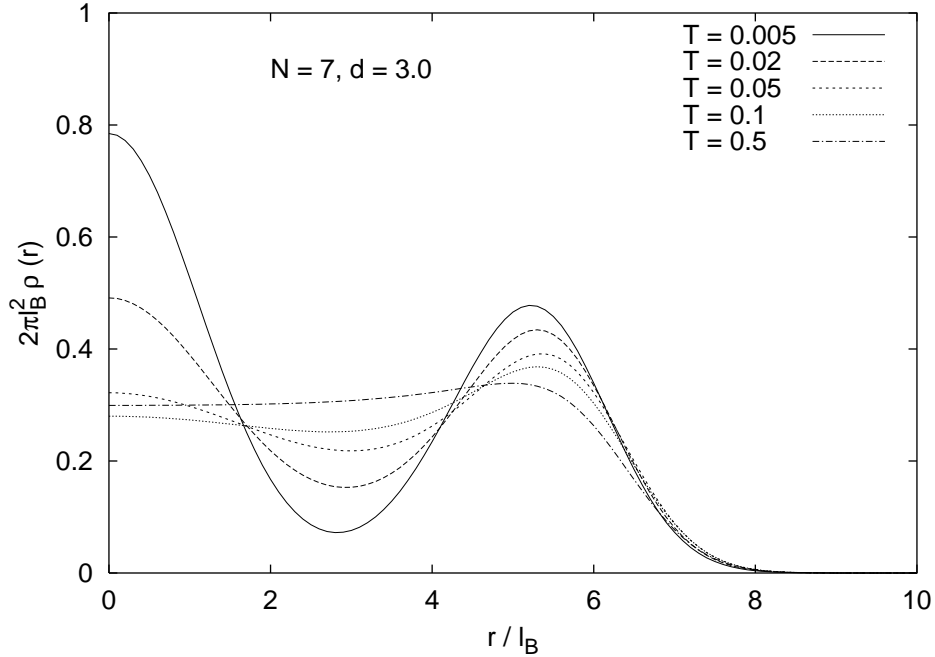


FIG. 9: Finite-temperature (in unit of  $e^2/\epsilon l_B$ ) electron density profiles  $\rho(r)$  for  $N = 7$  electrons at  $\nu = 1/3$ . The distance between the two charge layers is fixed at  $d = 3l_B$ . At and above  $T = 0.05e^2/\epsilon l_B$ ,  $\rho(r)$  become similar to that of the corresponding Laughlin state, fluctuating slightly around  $1/3$ . This is very different from  $\rho(r)$  at  $T = 0.005e^2/\epsilon l_B$ , where strong density oscillation due to edge reconstruction can be seen.

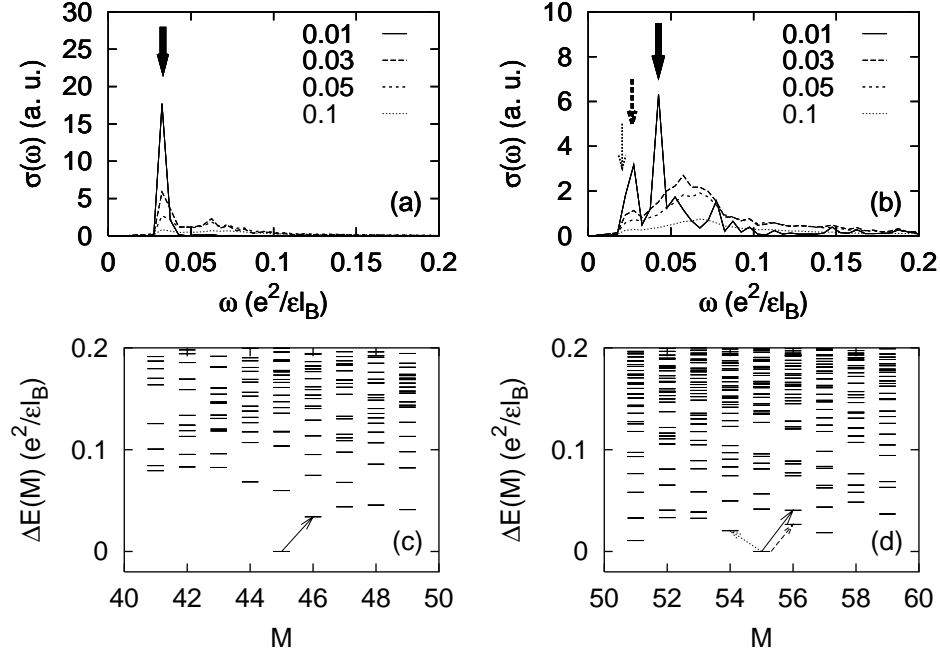


FIG. 10: Microwave conductivity  $\sigma(\omega)$  calculated by electric dipole spectral function for  $N = 6$  electrons at  $\nu = 1/3$  for (a)  $d = 1.0l_B$  (with no edge reconstruction) and (b)  $d = 2.0l_B$  (after edge reconstruction) at various temperatures. The corresponding low-energy excitation spectra are plotted for (c)  $d = 1.0l_B$  and (d)  $d = 2.0l_B$ . Before edge reconstruction, the absorption is dominated by long wave-length chiral edge mode [solid arrows in (a) and (c)] even above  $T = 0.05e^2/\epsilon l$ . After reconstruction, extra modes [indicated by three arrows in (b) and (d)] due to reconstructed edge can be identified as contributing to the peaks in  $\sigma(\omega)$  for  $\omega < 0.05$ , in units of  $e^2/\epsilon l$ . At  $T > 0.03e^2/\epsilon l$ , these modes become less significant, compared to bulk excitation.

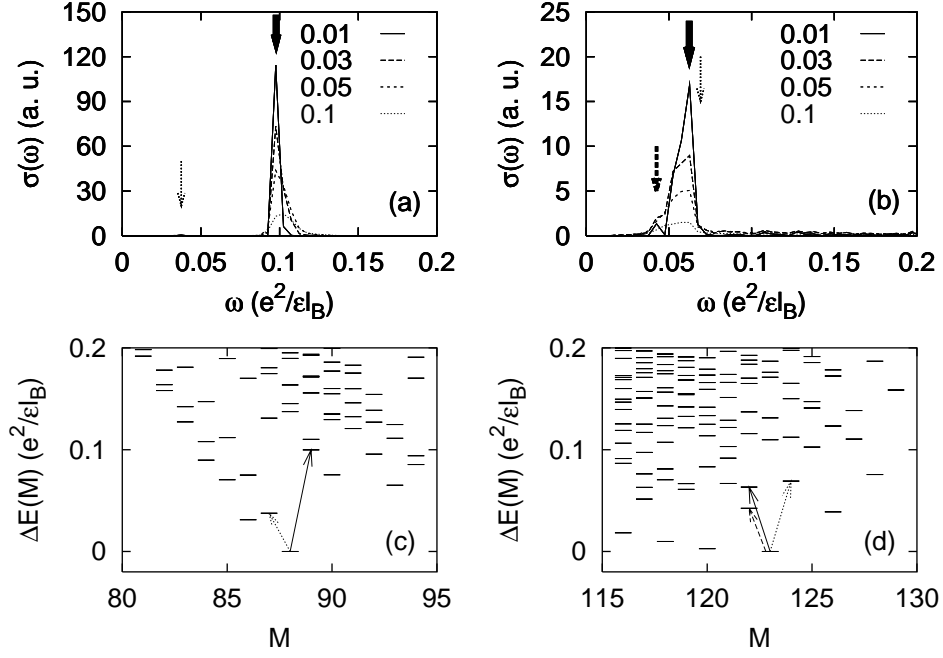


FIG. 11: Microwave conductivity  $\sigma(\omega)$  calculated by electric dipole spectral function for  $N = 12$  electrons at  $\nu = 2/3$  for (a)  $d = 0.1l_B$  and (b)  $d = 2.0l_B$  at various temperatures. The corresponding low-energy excitation spectra are plotted for (c)  $d = 0.1l_B$  and (d)  $d = 2.0l_B$ . For  $d = 0.1l_B$ ,  $\sigma(\omega)$  is dominated by the lowest  $\Delta M = +1$  edge mode [solid arrows in (a) and (c)], while the lowest  $\Delta M = -1$  edge mode [dotted arrows in (a) and (c)] is significantly weaker. For  $d = 2.0l_B$ ,  $\sigma(\omega)$  is dominated by the second lowest  $\Delta M = -1$  edge mode [solid arrows in (b) and (d)]. Both the lowest  $\Delta M = \pm 1$  modes are much weaker, as indicated by dashed and dotted arrows in (b) and (d).

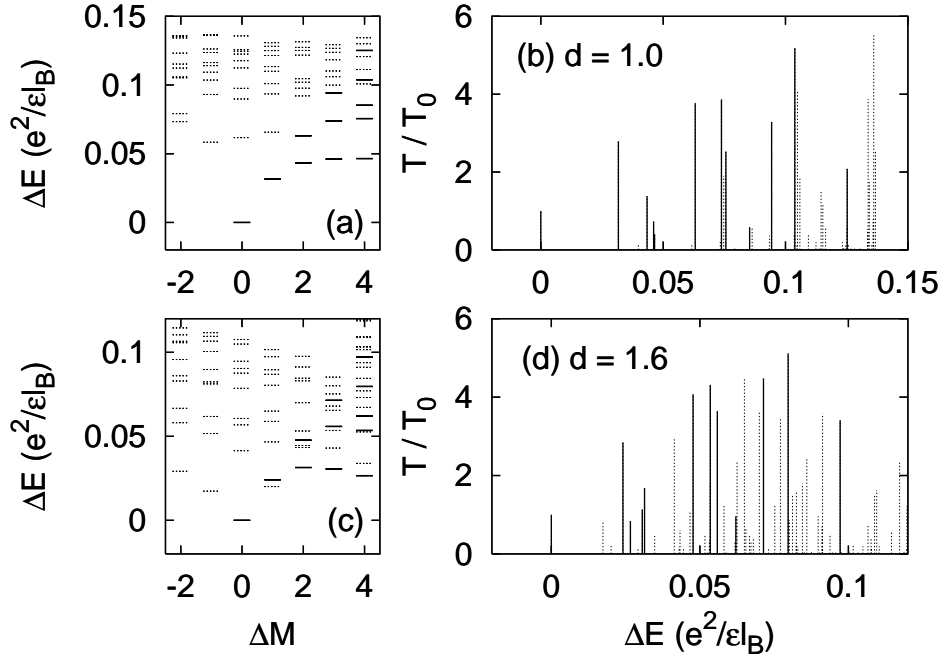


FIG. 12: (a) Spectrum and (b) normalized spectral weights,  $T(\{n_i\})/T_0$ , for tunneling one additional electron into a 6-electron system at  $\nu = 1/3$  for  $d = 1.0l_B$ . (c) Spectrum and (d) normalized spectral weights,  $T(\{n_i\})/T_0$ , for tunneling one additional electron into a 6-electron system at  $\nu = 1/3$  for  $d = 1.6l_B$ . In all figures, solid lines represent states that have significant contribution to the electron spectral function, whose corresponding matrix elements are listed in Table II.